JOURNAL OF NANO- AND ELECTRONIC PHYSICS
Vol. **9** No 3, 03025(5pp) (2017)

ЖУРНАЛ НАНО- ТА ЕЛЕКТРОННОЇ ФІЗИКИ
Том **9** № 3, 03025(5cc) (2017)

Study of Structural Evolution and Magnetic Behavior of $Ni_{50}Mn_{45}Sn_5$ Alloy

Dinesh Saini[1,*], Satyavir Singh[1], MK Banerjee[2,3], K. Sachdev[1,3]

[1] *Department of Physics, Malaviya National Institute of Technology Jaipur-302017, India*
[2] *Department of Metallurgical & Materials Engineering, Malaviya National Institute of Technology Jaipur-302017, India*
[3] *Materials Research Centre, Malaviya National Institute of Technology Jaipur-302017, India*

(Received 02 February 2017; published online 30 June 2017)

In this investigation, $Ni_{50}Mn_{45}Sn_5$ alloy powder is synthesized by employing mechanical alloying technique in a high energy planetary ball mill. Systematic study on microstructural evolution and magnetic properties after different milling time is conducted by X-ray Diffraction (XRD), Scanning Electron Microscope (SEM), Transmission Electron Microscope (TEM) and Vibrating Sample Magnetometer (VSM). It is revealed that formation of single phase alloy with an average of ~ 7 nm crystallite size is achieved after 20 hr milling by mechanically induced inter-diffusion of atoms. Moreover, changes in lattice parameters and lattice strain as a function of milling time is also studied. Change in morphology of particles with increasing milling time has been studied by SEM. In addition, d-spacing and diffraction planes obtained from analysis of HRTEM image and SAD pattern respectively corroborate with XRD results. Low coercivity indicated by hysteresis loop is suggestive of soft ferromagnetic behavior of the alloy powder.

Keywords: Alloy $Ni_{50}Mn_{45}Sn_5$, Structural evolution, Magnetic properties.

DOI: 10.21272/jnep.9(3).03025 PACS number: 81.05.Bx

1. INTRODUCTION

Heusler based ferromagnetic shape memory alloys Ni-Mn-X (X = Sn, Sb, In, Ga) have received considerable attention as smart materials due to their multifunctional properties viz. magnetic superelasticity [1], magnetocaloric effect [2, 3] and large magnetoresistance [4]. In particular, NiMnGa alloy has been the most extensively studied system over the past few years. However, due to some of the problems of Ga based alloys (such as high cost of Gallium, toxic nature, brittleness, low martensitic transformation temperature) limits their practical applications [5]. To conquer these disadvantages, development of Ga-free alloy is required. Alternatively, Ni-Mn-Sn Heusler alloy has become a choice of research because of its properties viz-a-viz low cost, non-toxicity, good ductility and high martensitic transformation temperature etc. [6, 7].

In recent years, a lot of researches [5, 8-10] have been done so far on the variety of methods of the alloy preparation. Several synthesis methods such as arc melting, melt spinning and spark erosion have been used to synthesize such alloys. Arc melting technique [5, 10-12] has been commonly used for the synthesis of NiMnX Heusler alloys but the alloys produced by this technique are usually brittle presumably due to coarse grains. Another major issue with arc melting technique is that it is difficult to maintain alloy composition because Mn is extremely volatile compound which causes the smelting loss. Although alloys prepared by melt-spinning [13-16] technique shows enhanced ductility due to smaller grain size, this technique is suitable for preparation of only ribbons [17]. From the application point of view, the fine powders into desired consolidated shapes are technologically much important for the fabrication of magnetocaloric devices [18]. Therefore, powder metallurgical routes has grown up as the most potential methods for improving the ductility of alloys, especially when there are reports in favor of improvements of not only ductility but also shape memory properties [19, 20]. In recent years, mechanical alloying (MA) has been considerably used to synthesize Heusler alloys because of its simplicity, cost effectiveness and high productivity for industrial scale applications [21]. In the present work, we have synthesized Ni50Mn45Sn5 alloy by using mechanical alloying technique instead of traditional melting methods. Efforts have been made to unveil the structural transformation and microstructural changes arising during mechanical alloying. The magnetic behavior of finally obtained powder after 20 hr milling has been studied. The major significance of this investigation lies in the fact that it will add to the existing knowledge in the understanding of various aspects of mechanical alloying for NiMn based Heusler alloys.

2. EXPERIMENTAL PROCEDURE

$Ni_{50}Mn_{45}Sn_5$ alloy was synthesized by a planetary ball milling machine (Fritsch Pulverisette P6), using Tungsten carbide (WC) (vial and balls), and nickel powder (Alfa Aesar-99.5%), Mn powder (Alfa Aesar-99.8%) and Sn powder (Alfa Aesar-99.9%). WC balls with 10 mm diameter and vial with 250 ml volume were used for milling purpose. Ball to powder (BPR) weight ratio was kept constant as 10:1. 50 WC balls were loaded into vial with 8 gm weight of each ball. Accordingly in order to maintain 10:1 ball to powder weight ratio, absolute 40 gm of powder was processed in a batch. The process was carried out at ambient temperature with a speed of 300 RPM. Milling was conducted in presence of Toluene (process controlling agent) to avoid excessive cold welding and oxidation of powder at room temperature. Powder samples were

* dineshsatrawla@yahoo.com

extracted after 0 hr, 2 hr, 6 hr, 12 hr and 20 hr milling to look into the progress of alloy formation. X-ray diffraction measurements were carried out for all the samples at room temperature, using Xpert-Pro Pan Analytical diffractometer (Cu K_α radiation). Average crystallite size and lattice-strain generated during milling were calculated through Williamson Hall formula. The morphology and particle size of the milled powders were analyzed by FESEM (Nova Nano FESEM 450 FEI). HRTEM image and SAD pattern of 20 hr milled powder sample were obtained by TEM (Technai 20 FEI). The magnetic properties of the 20 hr milled powder were measured by VSM (PPMS cryogenics limited USA) at room temperature.

3. RESULTS AND DISCUSSION

Fig. 1 displays X-ray diffraction patterns of powders milled for various times. Diffraction peaks for 0 hr milled powder mixture can be assigned to Ni (fcc) [JCPDF Card- 00-004-0850], Mn (bcc) [JCPDF Card- 00-032-0637] and Sn (tetragonal) [JCPDF Card- 00-004-0673]. XRD pattern corresponding to 2 hr milled powder did not undergo any major structural transformation.

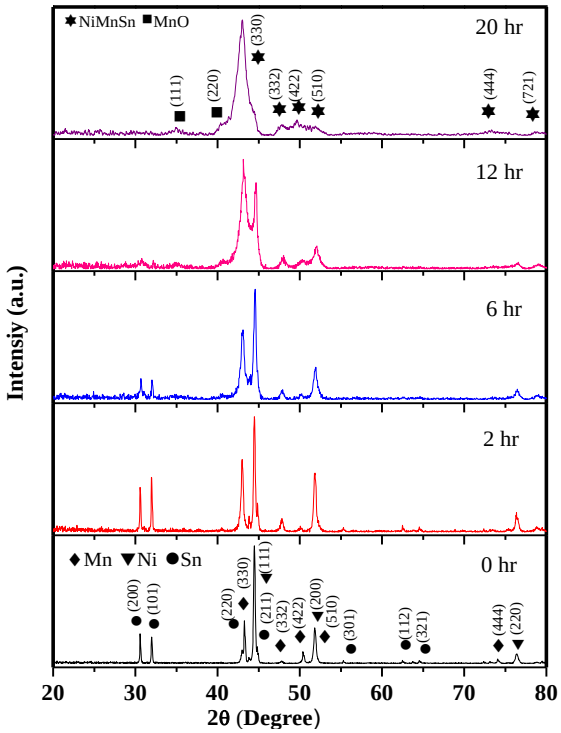

Fig. 1 – XRD diffraction patterns of powder milled for different times

Elemental diffraction peaks of precursor materials are still observed; this stage is known as early stage of milling. At this stage of milling, diffraction peaks are sharp. After 6 hr of milling, broadening of Bragg diffraction peaks is observed which indicates continuous refinement of particles as milling progresses. Simultaneously, there is a considerable decrease in intensity of diffraction peaks of Sn which is due to dissolution of Sn. After continuous milling up to 12 hr, intensity of Ni (111) peak decreases whereas intensity of Mn (330) peak increases which indicates mutual dissolution of Ni and Mn atoms into each other's lattice. Disappearance of Bragg diffraction peaks of Sn indicates complete dissolution of Sn. After 20 hr, all elemental Bragg diffraction peaks are disappeared which means that mechanical alloying is completed and the obtained diffraction pattern is indexed as NiMnSn alloy with BCC crystal structure. This is to be noted that no extra peaks belonging to any unwanted compounds were detected except minor oxidation of manganese.

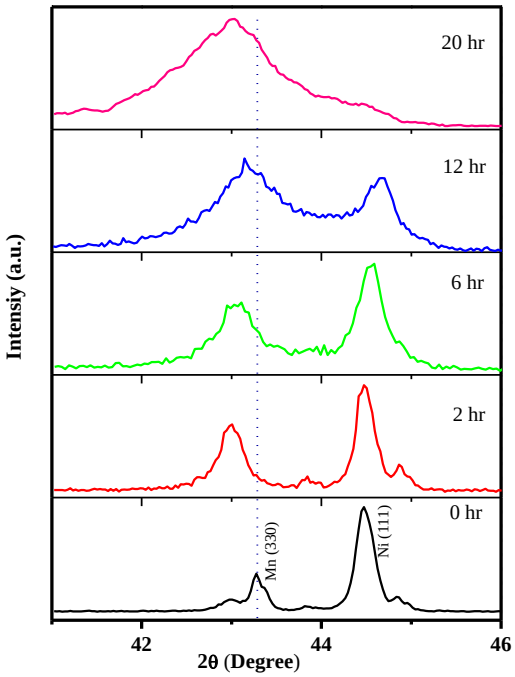

Fig. 2 – XRD peak shifting and broadening with milling time

Fig. 2 shows effect of milling time on the peak positions and peak width of the diffraction lines falling in the range of $2\theta = 41°$-$46°$. 0 hr milled powder mixture consists of Mn (330) and Ni (111) diffraction peaks in this range. Between 2 hr to 6 hr of milling, diffraction peaks are broadened and Mn (330) peak shifts towards lower degree of reflection. Broadening of diffraction peaks with increasing milling time occurs due to effective size reduction, increasing of lattice distortions and microstrain introduced by milling [22] whereas, shifting of Mn (330) peak towards lower degree is attributed to increase in interplanar spacing and hence lattice parameter due to continuous dissolution of Sn. Since the atomic diameter of Sn is 1.62 Å [23] which is larger than Mn 1.26 Å [23], therefore, dissolution of Sn induces distortion in the lattice which increases lattice parameter of Mn. In the duration of 6 hr to 20 hr milling, lattice parameter changes non monotonically which can be ascribed to the fact that atomic radii of Ni (1.24 Å) [23] and Mn (1.26 Å) are very close to each other therefore mutual dissolution of Mn and Ni into crystal structure of each other forming Ni-Mn and Mn-Ni is possible. Such dissolution does not change the lattice parameter and peak shifting significantly due to minor difference in atomic radii of Ni and Mn. After 20 hr milling, Ni (111) peak is disappeared and a single broad peak of NiMnSn alloy is formed. Table 1 summarizes

lattice parameters calculated by utilizing the Bragg's law for a cubic system [24]:

$$d = \frac{a}{\sqrt{h^2 + k^2 + l^2}} \quad (1)$$

where d is interplaner distance of (h k l) planes and a is lattice parameter.

Table 1 – Variation in lattice parameters with milling time

Milling time (hr)	Lattice Parameter (Å)
0	8.89
2	8.91
6	8.92
12	8.90
20	8.91

Fig. 3 illustrates the variation in crystallite size (D) and lattice-strain (ε) with milling time calculated by using Williamson-Hall equation [25]. As milling time increases, crystallite size becomes finer and reaches to ~ 7 nm after 20 hr. This refinement is brought by high speed collisions between ball-powder-ball and ball-powder-bowl converting larger size particles into finer ones. Refinement increases uniformly with the milling time and is more dominant during initial few hours of milling [26]. The lattice strain increases gradually and finally reaches to 1.4%. Typically, the lattice strain increases with rising milling time. As milling progresses, fraction of grain boundaries and dislocation density increases which results in an increase in lattice strain [27].

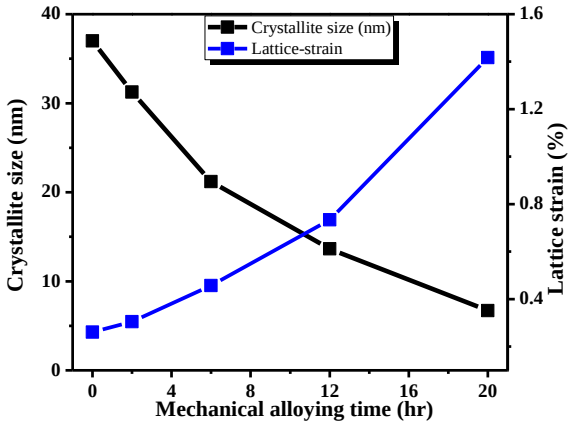

Fig. 3 – Variation in crystallite size and lattice strain with milling time

Fig. 4a elucidates the morphology of elemental powder mixture without milling with an average particle size 20-25 μm. Ni particles have round shape while the Mn and Sn particles have polygonal and oval shape respectively. As alloying progresses, continuous change in morphology and average particle size is noticed. Just after 2 hr, powder particles become irregular in shape along with 6-8 μm average particle size (Fig. 4b). During initial hours of milling a very high rate of ball-powder-ball collisions is primarily responsible for rapid decrease in particle size. After 6 hr, the powder particles get flattened to platelet shapes (Fig. 4c) due to the development of compressive forces by virtue of micro-forging. The average particle size at this stage was obtained 9-11 μm. This stage of milling incorporates both the cold welding and micro-forging processes simultaneously; therefore increase in particle size was noticed. After 12 hr, powder particles are work hardened therefore fracturing process becomes more prominent consequently; the average particle size at this stage was decreased and found 7-9 μm (Fig. 4d). Prolonged milling up to 20 hr produced more refined particles with an average particle size 5-8 μm (Fig. 4e).

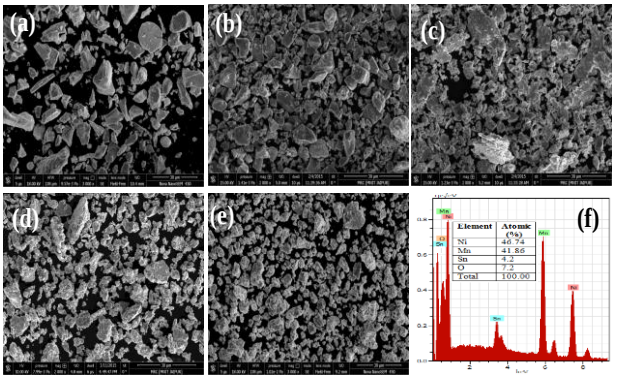

Fig. 4 – SEM micrographs of as-milled $Ni_{50}Mn_{45}Sn_5$ powder (a) 0 hr (b) 2 hr (c) 6 hr (d) 12 hr (e) 20 hr (f) EDS spectrum

SEM-EDS spectrum of 20 hr milled powder (Fig. 4f) shows that the composition of finally obtained alloy powder does not contain any other metallic contamination from the milling media. However, low percentage of oxygen was detected. Introduction of oxygen may be explained by oxidation of Mn particles on the surface during mechanical alloying process which corroborates to XRD results.

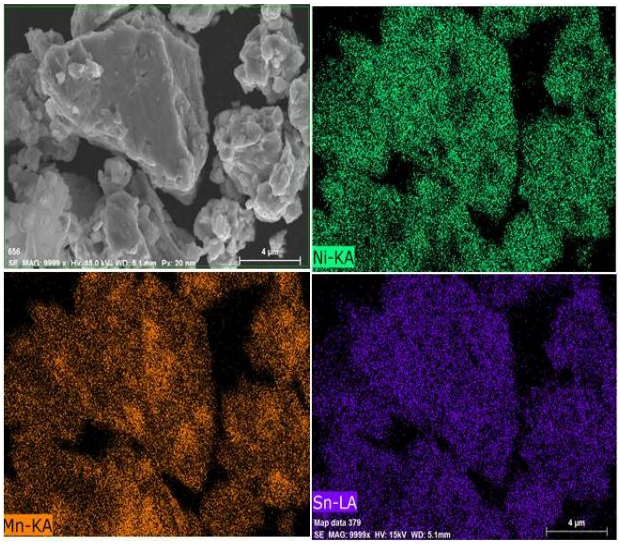

Fig. 5 – Secondary electron image of 20 hr milled powder

Secondary electron image (Fig. 5) shows elemental mapping of 20 hr milled alloy powder indicating homogeneous distribution of elements in alloy powder. Ni, Mn and Sn atoms distributions are closely correlated suggesting that three elements are almost completely alloyed which is an evidence of true alloy formation [28]. These results are very consistent with that of

XRD analysis. Fig. 6a and b shows TEM bright field image and the corresponding selected area diffraction (SAD) pattern of 20 hr milled alloy powder respectively. Figure 6a shows a collection of particles from which the average crystallite size was estimated between ~ 10-15 nm. SAD pattern exhibits diffraction rings for the (330), (332), (422) and (510) planes of the bcc crystal structure. Diffraction rings were indexed by measuring the distance from the centre of the diffraction pattern. In addition, HRTEM image is shown in Fig. 6c, for clear visibility of lattice fringes, an enlarged view of an area enclosed by rectangle in HRTEM image is presented in Fig. 6d, which was further processed by Digital-micrograph software to calculate the d-spacing ($d = 2.14$ Å) (see Fig. 6e). This value agrees well with d-spacing (2.12 Å) obtained from X-ray diffraction analysis. d-spacing was calculated by generating an IFFT profile plot and manually count the cycles, then divide the distance (2.14 nm) by the total number of cycles (10) as illustrated in Fig. 6f. Thus, TEM study shows that the analysis of SAD pattern and the crystallite size obtained through HRTEM are quite consistent with the XRD analysis.

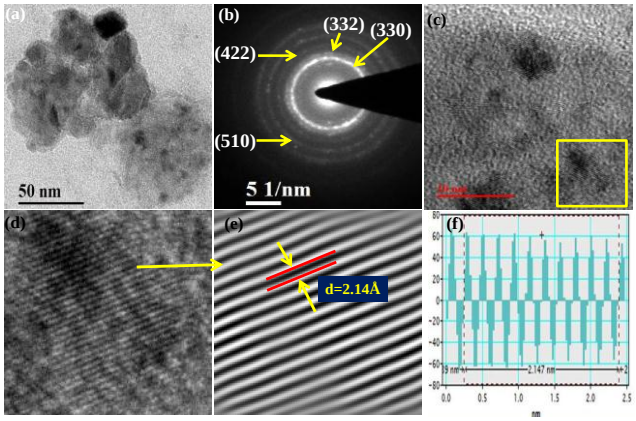

Fig. 6 –TEM images of 20 hr milled powder: (a) Bright field image of powder particles, (b) SAD pattern, (c) HRTEM image, (d) Enlarged view of rectangular area shown in image c, (e) Lattice fringes with calculated d-spacing, (f) IFFT profile

Fig. 7a shows magnetization curve of 20 hr milled powder as a function of field (-10 kOe ≤ H ≤ +10 kOe) at room temperature. The associated magnetic properties such as saturation magnetization (M_s), coercivity (H_c) and remanent magnetization (M_R) are deduced from the hysteresis loop and summarized in Table 2. It can be seen that the 20 hr milled powder sample exhibits a typical soft ferromagnetic behavior with saturation magnetization ($M_s = 4.25$ emu/gm) at ~ 10 kOe. Low value of saturation magnetization is due to ball milling which induces severe atomic disordering through the movement of dislocations and disturbs the position of Mn sites in the lattice, destructing the total magnetic moment [29]. It is known that magnetic moment in NiMn based Heuslar alloys originate from the exchange interaction between Mn atoms. Magnetic properties of the obtained ball milled alloy powder can be recovered by further heat treatment at appropriate temperature as shown by Tian et.al. [30]. Heat treatment process restores the magnetic moment in the alloy by promoting the atomic ordering of atoms.

Table 2 – Magnetic properties of 20 hr milled alloy powder

M_s	H_c	M_R	M_{sp}
4.25 emu/gm	237.38 Oe	1.18 mu/gm	14.06 mu/gm

To investigate the attributes of ground state magnetism, a virgin plot of $M(H)$ was drawn in the form of Arrott plot M^2 versus H/M [11]. The intersection point on positive M^2 axis indicates the presence of spontaneous magnetization (M_{sp}) in the system [31]. Fig. 7b illustrates Arrott plot, where a positive intercept on the M^2 axis gives spontaneous magnetization (M_{sp}) 14.06 emu/gm which suggests presence of ferromagnetic ordering in the present alloy system. After successful heat treatment, the obtained alloy has great possibility to be used as potential ferromagnetic shape memory alloy for different applications.

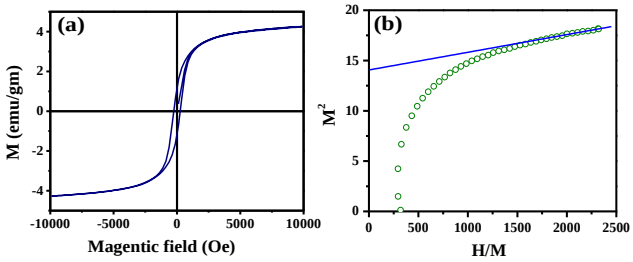

Fig. 7 –(a) Magnetization hysteresis loop of 20 hr milled powder (b) Arrott plot (M^2 versus H/M)

4. CONCLUSIONS

Single phase NiMnSn alloy powder with significant homogeneity was prepared by ball milling method. Parameters of ball milling reaction were optimized in such a way that no metallic contamination was observed from milling balls and bowl. It was found that lattice strain increased with milling time with concurrent decrease in crystallite size. Change in average particle size and modification in morphology of powder particles at different stages of milling was detected by SEM micrographs. Formation of single phase alloy powder after 20 hr milling was confirmed by TEM analysis. Narrow hysteresis curve indicating low value of coercivity with significant spontaneous magnetization makes the present alloy useful as soft ferromagnetic materials. The results of the present work suggest that ball milling is an effective way to produce contamination free single phase magnetic shape memory alloys.

AKNOWLEDGEMENTS

Authors are highly grateful to Materials Research Centre, MNIT Jaipur for providing the characterization facilities (XRD, SEM and TEM). Authors also thank JNU New Delhi for VSM facility.

REFERENCES

1. T. Krenke, E. Duman, M. Acet, EF. Wassermann, X. Moya, L. Manosa, L. Planes, E. Suard, B. Ouladdiaf, *Phys. Rev. B* **75**, 104414 (2010).
2. V.K. Sharma, M.K. Chattopadhyay, R. Kumar, T. Ganguli, P. Tiwari, S.B. Roy, *J. Phys.: Condens. Mat.* **20**, 425210 (2008).
3. V. Recarte, JI Pérez-Landazábal, S. Kustov, E. Cesari, *J. Appl. Phys.*, **107**, 053501 (2010).
4. K. Koike, M. Ohtsuka, Y. Honda, H. Katsuyama, M. Matsumoto, K. Itagaki, Y. Adachi, H. Morita, *J. Magn. Magn. Mater.* **310**, e996 (2007).
5. R. Coll, L. Escoda, J. Saurina, J.L. Sanchez-Llamazares, B. Hernando, J.J. Sunol, *J. Therm. Anal. Calorim.* **99**, 905 (2010).
6. S. Chatterjee, S. Giri, S.K. De, S. Majumdar, *Adv. Mater. Research.* **52**, 215 (2008).
7. P.J. Brown, A.P. Gandy, K. Ishida, R. Kainuma, T. Kanomata, K.U. Neumann, K. Oikawa, B. Ouladdiaf, K.R.A. Zeibeck, *J. Phys.: Condens. Matter.* **18**, 2249 (2006).
8. C. Jing, Y.J. Yang, Z. Li, X.L. Wang, B.J. Kang, S.X. Cao, J.C. Zhang, J. Zhu, B. Lu, *J. Appl. Phys.* **113**, 173902 (2013).
9. Y. Sutou, Y. Imano, N. Koeda, T. Omori, R. Kainuma, K. Ishida, K. Oikawa, *Appl. Phys. Lett.* **85**, 4358 (2004).
10. F. Chen, Y.X. Tong, B. Tian, L. Li, Y.F. Zheng and Y. Liu, *J. Magn. Magn. Mater.* **347**, 72 (2013).
11. A.K. Nayak, K.G. Suresh, A.K. Nigam, *J. Appl. Phys.* **107**, 09A927 (2013).
12. B. Gao, J. Shen, F.X. Hu, J. Wang, J.R. Sun, B.G. Shen, *Appl. Phys. A*, **97**, 443 (2009).
13. J.K. Yu, H.W. Li, Q.J. Zhai, J.X. Fu, Z.P. Luo, H.X. Zheng, *Adv. Manuf.* **2**, 353 (2014).
14. J.D. Santos, T. Sanchez, P. Alvarez, M.L. Sanchez, J.L. Sánchez Llamazares, B. Hernando, *J. Appl. Phys.* **103**, 07B326 (2008).
15. F. Chen, Y.X. Tong, Y.J. Huang, B. Tian, L. Li, Y.F. Zheng, *Intermetallics* **36**, 81 (2013)
16. B. Hernando, J.L. Sánchez Llamazares, J.D. Santos, Ll. Escoda, J.J. Suñol, R. Varga, D. Baldomir, D. Serantes, *Appl. Phys. Let.* **92**, 042504 (2008).
17. K. Ito, W. Ito, R.Y. Umetsu, S. Tajima, H. Kawaura, R. Kainuma, K. Ishida, *Scripta Mater.* **61**, 504 (2009).
18. I. Babita, S.I. Patil, S. Ram, *J. Phys. D: Appl. Phys.* **43**, 205002 (2010).
19. R.B. Perez-Saez, V. Recarte, M.L. No, O.A. Ruano, J. San Juan, *Adv. Eng. Mater.* **2**, 49 (2000).
20. X.H. Tian, J.H. Sui, X. Zhang, X. Feng, W. Cai, *J. Alloy. Compd.* **509**, 4081 (2011).
21. Kh. Gheisari, Sh. Shahriari, S. Javadpour, *J. Alloy. Compd.* **574**, 71 (2013).
22. C. Suryanarayana, *Prog. Mater. Sci.* **46**, 1 (2001).
23. P. Lázpita, J.M. Barandiarán, V.A. Chernenko, B. Valle García, E. Díaz Tajada, T. Lograsso, D.L. Schlagel, *J. Alloy. Compnd.* **594**, 171 (2014).
24. M. Abbasi, S.A. Sajjadi, M. Azadebh, *J. Alloy. Compd.* **497**, 171 (2010).
25. M. Hakimi, P. Kameli, H. Salamati, *J. Magn. Magn. Mater.* **322**, 3443 (2010).
26. H. Ahmadian Baghbaderani, S. Sharafi, M. Delshad Chermahini, *Powder Technol.* **230**, 241 (2012).
27. Sh. asibi, H. Shokrollahi, L. Karimi, K. Janghorban, *Powder Technol.* **228**, 404 (2012).
28. N.Kr. Prasad, V. Kumar, *J. Mater. Sci.: Mater. Electron.* **26**, 10109 (2015).
29. B. Tian, F. Chen, Y. Liu, Y.F. Zheng, *Intermetallics* **16**, 1279 (2008).
30. B. Tian, F. Chen, Y.X. Tong, L. Li, Y.F. Zheng, *JMEPEG* **21**, 2530 (2012).
31. I.N. Bhatti, R. Rawat, A. Banerjee, A.K. Pramanik, *J. Phys.: Condens. Matter* **27**, 016005 (2014).